

## ASTEROSEISMIC INVESTIGATION OF KNOWN PLANET HOSTS IN THE *KEPLER* FIELD

J. CHRISTENSEN-DALSGAARD<sup>1,2</sup>, H. KJELDEN<sup>1,2</sup>, T. M. BROWN<sup>3</sup>, R. L. GILLILAND<sup>4</sup>, T. ARENTOFT<sup>1,2</sup>, S. FRANDSEN<sup>1,2</sup>,  
P.-O. QUIRION<sup>1,2,5</sup>, W. J. BORUCKI<sup>6</sup>, D. KOCH<sup>6</sup>, AND J. M. JENKINS<sup>7</sup>

*Draft version November 15, 2018*

### ABSTRACT

In addition to its great potential for characterizing extra-solar planetary systems the *Kepler mission* is providing unique data on stellar oscillations. A key aspect of *Kepler* asteroseismology is the application to solar-like oscillations of main-sequence stars. As an example we here consider an initial analysis of data for three stars in the *Kepler* field for which planetary transits were known from ground-based observations. For one of these, HAT-P-7, we obtain a detailed frequency spectrum and hence strong constraints on the stellar properties. The remaining two stars show definite evidence for solar-like oscillations, yielding a preliminary estimate of their mean densities.

*Subject headings:* stars: fundamental parameters — stars: oscillations — planetary systems

### 1. INTRODUCTION

The main goal of the *Kepler mission* is to characterize extra-solar planetary systems, particularly Earth-like planets in the habitable zone (e.g., Borucki et al. 2009). The mission detects the presence of planets through the minute reduction of the light from a star as a planet crosses the line of sight. Several observations of such reductions at fixed time intervals for a given star, and extensive follow-up observations, are used to verify that the effect results from planet transits and to characterize the planet. To ensure a reasonable chance of detection *Kepler* observes more than 100,000 stars simultaneously, in a fixed field in the Cygnus-Lyra region. Most stars are observed at a cadence of 29.4 min, but a subset of up to 512 stars can be observed at a short cadence (SC) of 58.85 s. *Kepler* was launched on 6 March 2009 and data from the commissioning period and the first month of regular observations are now available.

The very high photometric accuracy required to detect planet transits (Borucki et al. 2010; Koch et al. 2010) also makes the *Kepler* observations of great interest for asteroseismic studies of stellar interiors. In particular, the SC data allow investigations of solar-like oscillations in main-sequence stars. Apart from the great astrophysical interest of such investigations they also provide powerful tools to characterize stars that host planetary systems (Kjeldsen et al. 2009).

In stars with effective temperature  $T_{\text{eff}} \lesssim 7000$  K we expect to see oscillations similar to those observed in the Sun (e.g., Christensen-Dalsgaard 2002), excited stochastically by the near-surface convection. These are acoustic modes of high radial order; in main-sequence stars such

modes approximately satisfy the asymptotic relation

$$\nu_{nl} \simeq \Delta\nu_0(n + l/2 + \epsilon) - l(l + 1)D_0 \quad (1)$$

(Vandakurov 1967; Tassoul 1980). Here  $\nu_{nl}$  is the cyclic frequency,  $n$  is the radial order of the mode and  $l$  is the degree,  $l = 0$  corresponding to radial (i.e., spherically symmetric) oscillations. Also,  $\Delta\nu_0$  is essentially the inverse sound travel time across the stellar diameter; this is closely related to the mean stellar density  $\langle\rho_*\rangle$ :  $\Delta\nu_0 \propto \langle\rho_*\rangle^{1/2}$ .  $D_0$  depends sensitively on conditions near the center of the star; for stars during the central hydrogen burning phase this provides a measure of stellar age. Finally,  $\epsilon$  is determined by conditions near the stellar surface. This regular form of the frequency spectrum simplifies the analysis of the observations, and the close relation between the stellar properties and the parameters characterizing the frequencies make them efficient diagnostics of the properties of the star. This has been demonstrated in the last few years through observations of solar-like oscillations from the ground and from space (for reviews, see Bedding & Kjeldsen 2008; Aerts et al. 2009; Gilliland et al. 2010a).

Even observations allowing a determination of  $\Delta\nu_0$  provide useful constraints on  $\langle\rho_*\rangle$ . With a reliable determination of individual frequencies  $\langle\rho_*\rangle$  is tightly constrained and an estimate of the stellar age can be obtained. This can greatly aid the interpretation of observations of planetary transits (e.g., Gilliland et al. 2010b; Nutzman et al. 2010). We note that photometric observations such as those carried out by *Kepler* are predominantly sensitive to modes of degree  $l = 0-2$ . As indicated by Eq. (1) these are sufficient to obtain information about the core properties of the star.

Ground-based transit observations have identified three planetary systems in the *Kepler* field: TrES-2 (O'Donovan et al. 2006; Sozzetti et al. 2007), HAT-P-7 (Pál et al. 2008), and HAT-P-11 (Dittmann et al. 2009; Bakos et al. 2010). These systems have been observed by *Kepler* in SC mode. Their properties (cf. Table 1) indicate that they should display solar-like oscillations at observable amplitudes, and hence they are obvious targets for *Kepler* asteroseismology. Here we report the results of a preliminary asteroseismic characterization of

arXiv:1001.0032v1 [astro-ph.SR] 30 Dec 2009

<sup>1</sup> Department of Physics and Astronomy, Aarhus University, DK-8000 Aarhus C, Denmark; e-mail jcd@phys.au.dk

<sup>2</sup> Danish AsteroSeismology Centre

<sup>3</sup> Las Cumbres Observatory Global Telescope, Goleta, CA 93117

<sup>4</sup> Space Telescope Science Institute, 3700 San Martin Drive, Baltimore, MD 21218

<sup>5</sup> Canadian Space Agency, 6767 Route de l'Aéroport, Saint-Hubert, QC, J3Y 8Y9 Canada (present address)

<sup>6</sup> NASA Ames Research Center, MS 244-30, Moffett Field, CA 94035, USA

<sup>7</sup> SETI Institute/NASA Ames Research Center, MS 244-30, Moffett Field, CA 94035, USA

TABLE 1  
PROPERTIES OF TRANSITING SYSTEMS.

Name	KIC No	$T_{\text{eff}}$ (K)	[Fe/H]	$L/L_{\odot}$	$\log(g)$ (cgs)	$v \sin i$ ( $\text{km s}^{-1}$ )	Source
HAT-P-7	10666592	$6350 \pm 80$	$0.26 \pm 0.08$	$4.9 \pm 1.1$	$4.07 \pm 0.06$	$3.8 \pm 0.5$	(a)
		$6525 \pm 61$	$0.31 \pm 0.07$		$4.09 \pm 0.08$		(b)
HAT-P-11	10748390	$4780 \pm 50$	$0.31 \pm 0.05$	$0.26 \pm 0.02$	$4.59 \pm 0.03$	$1.5 \pm 1.5$	(c)
TrES-2	11446443	$5850 \pm 50$	$-0.15 \pm 0.10$	$1.17 \pm 0.10$	$4.4 \pm 0.1$	$2 \pm 1$	(d)
		$5795 \pm 73$	$0.06 \pm 0.08$		$4.30 \pm 0.13$		(b)

NOTE. — Sources: (a): Pál et al. (2008); (b): Ammler-von Eif et al. (2009); (c): Bakos et al. (2010); (d): Sozzetti et al. (2007). In some cases asymmetric error bars have been symmetrized.

the central stars in the systems, based on the early *Kepler* data.

## 2. OBSERVATIONS AND DATA ANALYSIS

We have analyzed data from *Kepler* for three planet-hosting stars using a pipeline developed for fast and robust analysis of all *Kepler* p-mode data (Christensen-Dalsgaard et al. 2008; Huber et al. 2009). Each time series contains 63324 data points. SC data characteristics and minor post-pipeline processing are discussed in Gilliland et al. (2010c). In addition a limb-darkened transit light curve model fit has been removed and  $5\text{-}\sigma$  clipping applied to remove outlying data points from each of the time series. The frequency analysis contains four main steps:

1. We calculate an oversampled (factor of four) version of the power spectrum by using a least-squares fitting. We smoothed the spectrum to  $3\text{ }\mu\text{Hz}$  resolution to remove the fine structure caused by the finite mode lifetime.
2. We correlated the smoothed power spectrum with an equally spaced comb of delta functions, separated by  $\Delta\nu_0/2$ , and confined to a Gaussian-shaped band with a full width at half maximum of  $5\Delta\nu_0$ . We adopted the maximum of this convolution over lags between 0 and  $0.5\Delta\nu_0$  as the filter output for each  $\Delta\nu_0$ .
3. After identifying the peak correlation for the best matched model filter and extracting the large separation corresponding to this peak we calculate the *folded spectrum* (see Fig. 1b), i.e., the sum of the power as a function of frequency modulo the optimum large separation (the one corresponding to the peak correlation). The summed power is used to locate the p-mode structure and identify the ridges corresponding to the different mode degrees (based on the asymptotic relation).
4. From the asymptotic relation and the identification of mode degrees we finally identify the position of the individual p-mode frequencies in the smoothed version of the power spectrum; when more than one mode is seen near the expected frequency we use the power-weighted average of the two peaks. Those extracted frequencies and the mode identifications are used in the modeling.

For observations with low signal-to-noise ratio it may not be possible to identify the individual frequencies. In

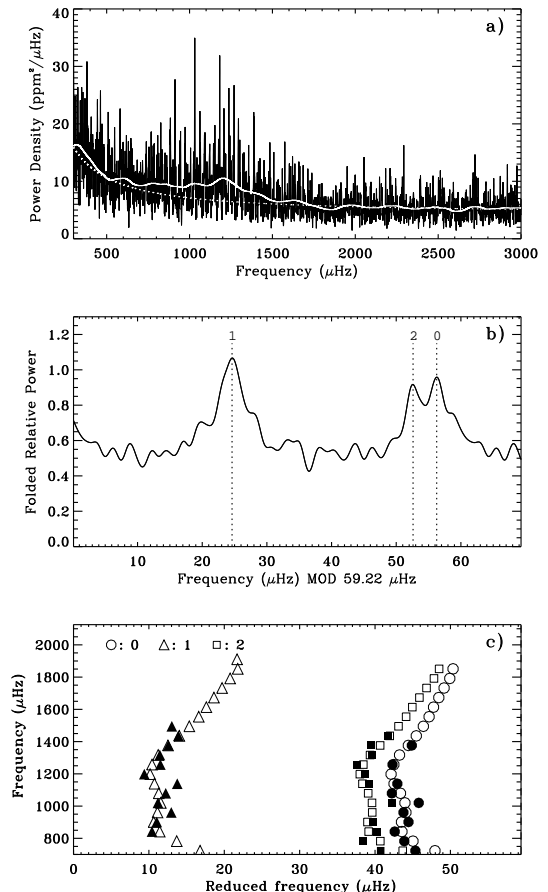


FIG. 1.— (a) Power spectrum of HAT-P-7 for frequencies between 300 and  $3000\text{ }\mu\text{Hz}$ . The spectrum is smoothed with a gaussian filter with a FWHM of  $3\text{ }\mu\text{Hz}$ . The noise level at high frequencies corresponds to  $1.1\text{ ppm}$  in amplitude. The white curve is a smoothed power spectrum with a gaussian filter ( $150\text{ }\mu\text{Hz}$  FWHM). A fit to the background (dashed white curve) is also shown. The excess power and the individual p-modes are evident. (b) Folded power spectrum, between  $750$  and  $1500\text{ }\mu\text{Hz}$ , for HAT-P-7 for a large separation of  $59.22\text{ }\mu\text{Hz}$ . Indicated are the positions corresponding to radial modes ( $l = 0$ ) and non-radial modes with  $l = 1$  and  $2$ . The measured positions are used to identify the individual oscillation modes in panel (a). (c) Échelle diagram (see text) for frequencies of degree  $l = 0, 1,$  and  $2$  in HAT-P-7; a frequency separation of  $59.36\text{ }\mu\text{Hz}$  and a starting frequency of  $10.8\text{ }\mu\text{Hz}$  were used. The filled symbols, coded for degree as indicated, show the observed frequencies, while the open symbols are for Model 3 in Table 2, minimizing  $\chi^2_{\nu}$ .

such cases the analysis is carried through step 2, to determine the maximum response and hence an estimate of the large separation.

Results on the three individual cases are presented in §4.

### 3. MODEL FITTING

Stellar evolution models and adiabatic oscillation frequencies were computed using the Aarhus codes (Christensen-Dalsgaard 2008a,b), with the OPAL equation of state (Rogers et al. 1996) and opacity (Iglesias & Rogers 1996) and the NACRE nuclear reaction parameters (Angulo et al. 1999). In some cases (see below) diffusion and settling of helium were included, using the simplified formulation of Michaud & Proffitt (1993). Convection was treated with the Böhm-Vitense (1958) mixing-length formulation, with a mixing length  $\alpha_{\text{ML}} = 2.00$  in units of the pressure scale height roughly corresponding to a solar calibration. In some models with convective cores, overshoot was included over a distance of  $\alpha_{\text{ov}}$  pressure scale heights. Evolution started from chemically homogeneous zero-age models. The initial abundances by mass  $X_0$  and  $Z_0$  of hydrogen and heavy elements were characterized by the assumed value of  $[\text{Fe}/\text{H}]$ , using as reference a present solar surface composition with  $Z_{\text{s}}/X_{\text{s}} = 0.0245$  (Grevesse & Noels 1993) and assuming, from galactic chemical evolution, that  $X_0 = 0.7679 - 3Z_0$ .

From the observed  $\Delta\nu_0$ , effective temperature and composition an initial estimate of the stellar parameters was obtained using the grid-based SEEK pipeline (Quirion et al., in preparation). Smaller grids were then computed in the vicinity of these initial parameters, to obtain tighter constraints on stellar properties. For HAT-P-7 the analysis of the observations yielded frequencies of individually identified modes; here the analysis was based on

$$\chi_{\nu}^2 = \frac{1}{N-1} \sum_{nl} \left( \frac{\nu_{nl}^{(\text{obs})} - \nu_{nl}^{(\text{mod})}}{\sigma_{\nu}} \right)^2, \quad (2)$$

where  $\nu_{nl}^{(\text{obs})}$  and  $\nu_{nl}^{(\text{mod})}$  are the observed and model frequencies,  $\sigma_{\nu}$  is the standard error in the observed frequencies (assumed to be constant) and  $N$  is the number of observed frequencies. In addition, we considered  $\chi^2 = \chi_{\nu}^2 + \chi_T^2$ , where  $\chi_T^2$  is the corresponding normalized square difference between the observed and model effective temperature. When  $\chi_{\nu}^2$  was available we minimized it along each evolution track and considered the resulting minimum values, and the corresponding value of  $\chi^2$ , as a function of the parameters characterizing the models (see Gilliland et al. 2010b, for details). When only the large separation  $\Delta\nu_0$  could be determined from the observations, we identified the model along each track which matched  $\Delta\nu_0$  and considered the resulting  $\chi_T^2$  as a function of the model parameters.

## 4. RESULTS

### 4.1. HAT-P-7

The observed power spectrum for HAT-P-7 is shown in Fig. 1a. The presence of solar-like p-mode peaks, with a maximum power around 1.1 mHz, is evident. At high frequency the noise level in the amplitude spectrum is

1.1 parts per million (ppm), with some increase at lower frequency, likely due to the effects of stellar granulation.

Carrying out the correlation analysis described in §2 we determined the large separation as  $\Delta\nu_0 = 59.22 \mu\text{Hz}$ . Figure 1b shows the resulting folded spectrum. This clearly shows two closely spaced peaks, identified as corresponding to modes of degree  $l = 0$  and 2, and single peak separated from these two by approximately  $\Delta\nu_0/2$ , corresponding to  $l = 1$ . On this basis we finally determined the individual frequencies, identifying the modes from the asymptotic relation; the final set includes 33 p-mode frequencies, determined with a standard error  $\sigma_{\nu} = 1.4 \mu\text{Hz}$ . These frequencies, corresponding to radial orders between 11 and 24, are illustrated in Fig. 1c in an échelle diagram (see below).

A grid of models was computed for masses between 1.41 and 1.61  $M_{\odot}$ ,  $[\text{Fe}/\text{H}]$  between 0.17 and 0.38, and  $\alpha_{\text{ov}} = 0, 0.1$  and 0.2, extending well beyond the end of central hydrogen burning. The modeling did not include diffusion and settling. At the mass of this star the outer convection zone is quite thin, and as a result the settling timescale is much shorter than the age of the star. Including settling, without compensating effects such as partial mixing in the radiative region or mass loss, leads to a rapid change in the surface composition which is inconsistent with the observed  $[\text{Fe}/\text{H}]$ ; for simplicity we therefore neglected these effects for HAT-P-7.<sup>8</sup>

The computed frequencies were corrected according to the procedure of Kjeldsen et al. (2008) for errors in the modeling of the near-surface layers, by adding  $a(\nu/\nu_0)^b$  where  $a = 0.1158 \mu\text{Hz}$ ,  $\nu_0 = 1000 \mu\text{Hz}$  and  $b = 4.9$ . As discussed in §3, for each evolution track, characterized by a set of model parameters, we minimized the departure  $\chi_{\nu}^2$  of the model frequencies from the observations, defining the best model for this set.

We first consider  $\chi_{\nu}^2$  as a function of the effective temperature of the models (Fig. 2a). It is evident that there is a clear minimum in  $\chi_{\nu}^2$ ; this is consistent with the determination of  $T_{\text{eff}}$  by Pál et al. (2008) but not with the somewhat higher temperature obtained by Ammler-von Eif et al. (2009) (see also Table 1). Thus in the following we use the observed quantities from Pál et al. (2008).

Since the frequencies to leading order are determined by the mean stellar density  $\langle\rho_{*}\rangle$ , Fig. 2b,c show  $\chi_{\nu}^2$  and  $\chi^2$  as functions of  $\langle\rho_{*}\rangle$ . It is evident that the best-fitting models occupy a narrow range of  $\langle\rho_{*}\rangle$ , with a well-defined minimum. Fitting a parabola to  $\chi^2$  in panel (c) we obtain the estimate  $\langle\rho_{*}\rangle = 0.2712 \pm 0.0032 \text{ g cm}^{-3}$ . In Fig. 2d  $\chi^2$  is shown against model age. Here the variation with model parameters is substantially stronger, resulting in a greater spread in the inferred age; in particular, it is evident, not surprisingly, that the results depend on the extent of convective overshoot. From the figure we estimate that the age of HAT-P-7 is between 1.4 and 2.3 Gyr.

Examples of evolution tracks are shown in Fig. 3; parameters for these models are provided in Table 2. They were chosen to give the smallest  $\chi_{\nu}^2$  for each of the three values of  $\alpha_{\text{ov}}$  considered. Also shown are the locations

<sup>8</sup> Artificially suppressing settling in the outer layers, while including diffusion and settling in the core, leads to results that are very similar to those presented here.

TABLE 2  
STELLAR EVOLUTION MODELS FITTING THE OBSERVED FREQUENCIES FOR HAT-P-7.

$N_o$	$M_*/M_\odot$	Age (Gyr)	$Z_0$	$X_0$	$\alpha_{ov}$	$R_*/R_\odot$	$\langle \rho_* \rangle$ ( $\text{g cm}^{-3}$ )	$T_{\text{eff}}$ (K)	$L_*/L_\odot$	$\chi_\nu^2$	$\chi^2$
1	1.53	1.758	0.0270	0.6870	0.0	1.994	0.2718	6379	5.91	1.08	1.21
2	1.52	1.875	0.0290	0.6809	0.1	1.992	0.2708	6355	5.81	1.04	1.04
3	1.50	2.009	0.0270	0.6870	0.2	1.981	0.2718	6389	5.87	1.00	1.24

NOTE. — Models minimizing  $\chi_\nu^2$  (cf. Eq. 2) along the evolution tracks, illustrated in Fig. 3. The models have been selected as providing the smallest  $\chi_\nu^2$  for each of the three values of the overshoot parameter  $\alpha_{ov}$ . The smallest value of  $\chi_\nu^2$  is obtained for Model 3.

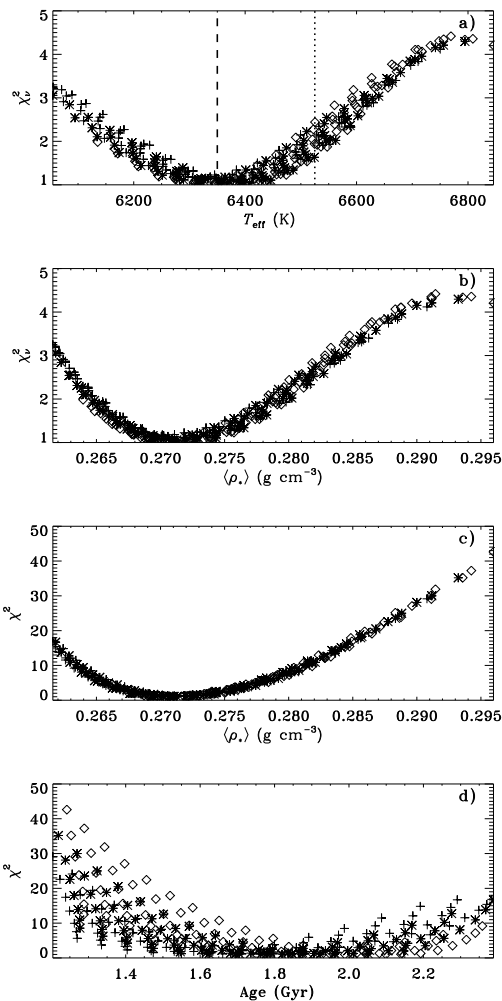


FIG. 2.— Results of fitting the observed frequencies to a grid of stellar models (see text for details). Pluses, stars and diamonds correspond to models with  $\alpha_{ov} = 0$  (no overshoot), 0.1, and 0.2. (a) Minimum mean square deviation  $\chi_\nu^2$  of the frequencies (cf. Eq. 2) along each evolution track, against the effective temperature  $T_{\text{eff}}$  of the corresponding models. The vertical dashed and dotted lines indicate the effective temperatures found by Pál et al. (2008) and Ammler-von Eif et al. (2009). (b) Minimum mean square deviation  $\chi_\nu^2$  against the mean density ( $\rho_*$ ) of the corresponding models. (c) As (b), but showing the combined  $\chi^2$ . (d)  $\chi^2$  against the age for the models that minimize  $\chi_\nu^2$ ; the different ridges correspond to the different masses in the grid, the more massive models resulting in a lower estimate of the age.

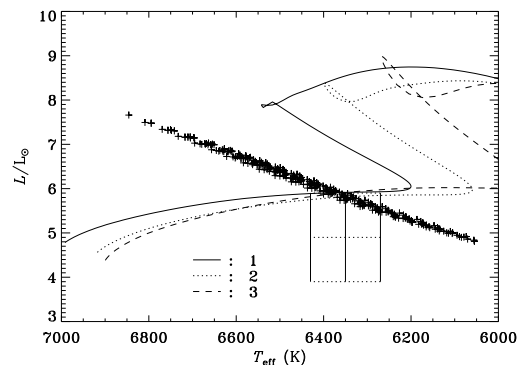


FIG. 3.— Theoretical HR diagram with selected evolutionary tracks, corresponding to the models defined in Table 2. The '+' indicate the models along the full set of evolutionary sequences minimizing the difference between the computed and observed frequencies. The box is centered on the  $L$  and  $T_{\text{eff}}$  as given by Pál et al. (2008), with a size matching the errors on these quantities.

of the models minimizing  $\chi_\nu^2$  along each of the computed tracks; these evidently fall close to a line in the HR diagram, corresponding to the small range in  $\langle \rho_* \rangle$ . The range of luminosities, from Pál et al. (2008), is based on modeling and hence has not been used in our fit; even so, it is gratifying that the present models are essentially consistent with these values. Also, as indicated by Fig. 2a and Table 2, the best-fitting models are close to the value of  $T_{\text{eff}}$  obtained by Pál et al. (2008).

The match of the best-fitting model (Model 3 of Table 2) to the observed frequencies is illustrated in a so-called *échelle diagram* (Grec et al. 1983) in Fig. 1c. In accordance with Eq. (1) the frequency spectrum is divided into slices of length  $\Delta\nu$ , starting at a frequency of  $10.8 \mu\text{Hz}$ ; the figure shows the location of the observed (filled symbols) and computed (open symbols) frequencies within each slice, against the starting frequency of the slice; the model results extend to the acoustical cut-off frequency,  $1930 \mu\text{Hz}$ , of the model. There is clearly a very good overall agreement between model and observations, including the detailed variation with frequency which reflects the frequency dependence of the large separation, as a possible diagnostics of the outer layers of the star (e.g., Houdek & Gough 2007).

We have finally made a fit of the inferred  $\langle \rho_* \rangle$ , as well as  $T_{\text{eff}}$  and  $[\text{Fe}/\text{H}]$  from Pál et al. (2008), to computed evolutionary tracks from the Yonsei-Yale compilation (Yi et al. 2001). This was based on a Markov Chain Monte Carlo analysis to obtain the statistical properties of the inferred quantities (see Brown 2010, for details). This resulted in  $M = 1.520 \pm 0.036 M_\odot$ ,  $R = 1.991 \pm 0.018 R_\odot$  and an age of  $2.14 \pm 0.26 \text{ Gyr}$ . We note that the age estimate reflects the specific as-

sumptions in the Yonsei-Yale evolution calculations; as indicated by Fig. 2d the true uncertainty in the age determination is likely somewhat larger.

#### 4.2. HAT-P-11

For HAT-P-11 the oscillation amplitudes were much smaller than in HAT-P-7, as expected from the general scaling of amplitudes with stellar mass and luminosity (e.g., Kjeldsen & Bedding 1995). Thus with the present short run of data it has only been possible to determine the large separation  $\Delta\nu_0 = 180.1 \mu\text{Hz}$  from the maximum in the correlation analysis. We have matched this to a grid of models, including diffusion and settling of helium, with masses between 0.7 and 0.9  $M_\odot$  and  $[\text{Fe}/\text{H}]$  between 0.21 and 0.41. These models provide a good fit to the observed  $T_{\text{eff}}$  and  $L/L_\odot$ ; note that in the present case the luminosity is based on a reasonably well-determined parallax. We have determined an estimate of  $\langle\rho_*\rangle$  by averaging the results of those models which match the observed  $\Delta\nu_0$  and lie within 2 standard deviations ( $\pm 100$  K) from the value of  $T_{\text{eff}}$  provided by Bakos et al. (2010); the result is  $\langle\rho_*\rangle = 2.5127 \pm 0.0009 \text{ g cm}^{-3}$ . Although the formal error is extremely small, owing to a tight relation between the large separation and the mean density for stars in this region in the HR diagram, the true error is undoubtedly substantially larger. In particular, we neglected the error in the determination of  $\Delta\nu_0$  and these data have not allowed a correction for the systematic errors in the modeling of the near-surface layers of the star.

#### 4.3. TrES-2

Here also we were unable to determine individual frequencies from the present set of data. The expected amplitudes are smaller than for HAT-P-7, and the noise level higher due to the fainter magnitude of TrES-2. The correlation analysis yielded two possible values of  $\Delta\nu_0$ :  $97.7 \mu\text{Hz}$  and  $130.7 \mu\text{Hz}$ . For this star  $\langle\rho_*\rangle$  has been determined from the analysis of the transit light curve. Sozzetti et al. (2007) obtained  $\langle\rho_*\rangle = 1.375 \pm 0.065 \text{ g cm}^{-3}$ , while Southworth (2009) found  $\langle\rho_*\rangle = 1.42 \pm 0.13 \text{ g cm}^{-3}$ . From the scaling with  $\langle\rho_*\rangle^{1/2}$  the

smaller of the two possible values of  $\Delta\nu_0$  is clearly inconsistent with these values of  $\langle\rho_*\rangle$ , while  $\Delta\nu_0 = 130.7 \mu\text{Hz}$  yields models that are consistent with the observed  $T_{\text{eff}}$  and  $\log(g)$  of Sozzetti et al. (2007) as well as with these values of the mean density. Here we considered a grid of models with helium diffusion and settling, masses between 0.85 and 1.1  $M_\odot$  and  $[\text{Fe}/\text{H}]$  between  $-0.25$  and  $-0.05$ . Determining again the mean value of  $\langle\rho_*\rangle$  for those models that matched  $\Delta\nu_0$  and had  $T_{\text{eff}}$  within two standard deviations of the value of Sozzetti et al. (2007) we obtained  $\langle\rho_*\rangle = 1.3233 \pm 0.0027 \text{ g cm}^{-3}$ . As in the case of HAT-P-11 the true error is likely substantially higher.

## 5. DISCUSSION AND CONCLUSION

The present preliminary analysis provides a striking demonstration of the potential of *Kepler* asteroseismology and its supporting role in the analysis of planet hosts. These stars will undoubtedly be observed throughout the mission and hence the quality of the data will increase substantially. For HAT-P-7 the detected frequencies are already close to what will be required for a detailed analysis of the stellar interior, beyond the determination of the basic parameters of the star. Thus here we can look forward to a test of the assumptions of the stellar modeling; the resulting improvements will further constrain the overall properties of the star, in particular its age. Also, given the observed  $v \sin i$  we expect a rotational splitting comparable to that observed in the Sun, and hence likely detectable with a few months of observations. For the other two stars there is strong evidence for the presence of solar-like oscillations; thus continued observations will very likely result in the determination of individual frequencies and hence further constraints on the properties of the stars.

Funding for this Discovery mission is provided by NASA's Science Mission Directorate. We are very grateful to the entire *Kepler* team, whose efforts have led to this exceptional mission. The present work was supported by the Danish Natural Science Research Council.

*Facilities:* The Kepler Mission

## REFERENCES

- Aerts, C., Christensen-Dalsgaard, J., & Kurtz, D. W. 2009, *Asteroseismology*, Springer, Heidelberg, in the press
- Ammler-von Eif, M., Santos, N. C., Sousa, S. G., Fernandes, J., Guillot, T., Israelian, G., Mayor, M., & Melo, C. 2009, *A&A*, 507, 523
- Angulo, C., et al. 1999, *Nucl. Phys. A*, 656, 3
- Bakos, G. Á., et al. 2010, *ApJ*, in the press ([arXiv:0901.0282v2](https://arxiv.org/abs/0901.0282v2))
- Bedding, T. R., & Kjeldsen, H. 2008, in *Proc. 14<sup>th</sup> Cambridge Workshop on Cool Stars, Stellar Systems, and the Sun*, ed. G. T. van Belle, ASP Conf. Ser., San Francisco, 384, 21
- Böhm-Vitense, E. 1958, *ZAp*, 46, 108
- Borucki, W., et al. 2009, in *Proc. IAU Symp. 253, Transiting Planets*, eds F. Pont, D. Sasselov & M. Holman, IAU and Cambridge University Press, 289
- Borucki, W., et al. 2010, *Science*, submitted
- Brown, T. M. 2010, *ApJ*, in the press ([arXiv:0912.1639](https://arxiv.org/abs/0912.1639))
- Christensen-Dalsgaard, J. 2002, *Rev. Mod. Phys.*, 74, 1073
- Christensen-Dalsgaard, J. 2008a, *Ap&SS*, 316, 13
- Christensen-Dalsgaard, J. 2008b, *Ap&SS*, 316, 113
- Christensen-Dalsgaard, J., Arentoft, T., Brown, T. M., Gilliland, R. L., Kjeldsen, H., Borucki, W. J., & Koch, D. 2008, in *Proc. HELAS II International Conference: Helioseismology, Asteroseismology and the MHD Connections*, eds L. Gizon & M. Roth, *J. Phys.: Conf. Ser.*, 118, 012039
- Dittmann, J. A., Close, L. M., Green, E. M., Scuderi, L. J., & Males, J. R. 2009, *ApJ*, 699, L48
- Gilliland, R. L., et al. 2010a, *PASP*, in the press
- Gilliland, R. L., McCullough, P. R., Nelan, E. P., Brown, T. M., Charbonneau, D., Nutzman, P., Christensen-Dalsgaard, J., & Kjeldsen, H. 2010b, *ApJ*, submitted
- Gilliland, R. L., et al. 2010c, *ApJL*, in the press
- Greç, G., Fossat, E., & Pomerantz, M. 1983, *Sol. Phys.*, 82, 55
- Grevesse, N., & Noels, A. 1993, in *Origin and evolution of the Elements*, eds N. Prantzos, E. Vangioni-Flam & M. Cassé (Cambridge: Cambridge Univ. Press), 15
- Houdek, G., & Gough, D. O. 2007, *MNRAS*, 375, 861
- Huber, D., Stello, D., Bedding, T. R., Chaplin, W. J., Arentoft, T., Quirion, P.-O., & Kjeldsen, H. 2009, *Comm. in Asteroseismology*, 160, 74
- Iglesias, C. A., & Rogers, F. J. 1996, *ApJ*, 464, 943
- Kjeldsen, H., & Bedding, T. R. 1995, *A&A*, 293, 87

- Kjeldsen, H., Bedding, T. R., & Christensen-Dalsgaard, J. 2008, *ApJ*, 683, L175
- Kjeldsen, H., Bedding, T. R., & Christensen-Dalsgaard, J. 2009, in *Proc. IAU Symp. 253, Transiting Planets*, eds F. Pont, D. Sasselov & M. Holman, IAU and Cambridge University Press, 309
- Koch, D., et al. 2010, *ApJL*, submitted
- Michaud, G., & Proffitt, C. R. 1993, in *Proc. IAU Colloq. 137: Inside the stars*, eds A. Baglin, & W. W. Weiss, ASP Conf. Ser., San Francisco, 40, 246
- Nutzman, P., Gilliland, R. L., McCullough, P. R., Charbonneau, D., Christensen-Dalsgaard, J., Kjeldsen, H., Nelan, E. P., Brown, T. M., & Holman, M. J. 2010, *ApJ*, submitted
- O'Donovan, F. T., et al. 2006, *ApJ*, 651, L61
- Pál, A., et al. 2008, *ApJ*, 680, 1450
- Rogers, F. J., Swenson, F. J., & Iglesias, C. A. 1996, *ApJ*, 456, 902
- Southworth, J. 2009, *MNRAS*, 394, 272
- Sozzetti, A., Torris, G., Charbonneau, D., Latham, D. W., Holman, M. J., Winn, J. N., Laird, J. B., & O'Donovan, F. T. 2007, *ApJ*, 664, 1190
- Tassoul, M. 1980, *ApJS*, 43, 469
- Yi, S., Demarque, P., Kim, Y.-C., Lee, Y.-W., Ree, C. H., Lejeune, T., & Barnes, S. 2001, *ApJS*, 136, 417
- Vandakurov, Yu. V. 1967, *AZh*, 44, 786 (English translation: *Soviet Ast.*, 11, 630)